Effect of Conformational Heterogeneity on Excitation Energy Transfer Efficiency in Directly *meso*−*meso* Linked Zn(II) Porphyrin Arrays

Tae Kyu Ahn,[†,‡] Zin Seok Yoon,[†] In-Wook Hwang,[†] Jong Kuk Lim,[†,‡] Hanju Rhee,[§] Taiha Joo,[§] Eunji Sim,[†] Seong Keun Kim,[‡] Naoki Aratani,[||] Atsuhiro Osuka,*[,||] and Dongho Kim*[,†]

Department of Chemistry and Center for Ultrafast Optical Characteristic Control, Yonsei University, Seoul 120-749, Korea, School of Chemistry, Seoul National University, Seoul 151-747, Korea, Department of Chemistry, Pohang University of Science and Technology, Pohang 790-784, Korea, and Department of Chemistry, Kyoto University, Sakyo-ku, Kyoto 606-8502, Japan

Received: February 7, 2005; In Final Form: April 11, 2005

We have investigated the overall excitation energy relaxation dynamics in linear porphyrin arrays as well as the energy transport phenomena by attaching an energy acceptor to one end of a linear porphyrin array by using steady state and time-resolved spectroscopic measurements. We have revealed that the solvation dynamics as well as the conformational dynamics contributes significantly to the energy relaxation processes of linear porphyrin arrays. Consequently, long porphyrin arrays no longer serve as good energy transmission elements in donor−acceptor linked systems due to conformational heterogeneities which provide the nonradiative deactivation channels as energy quenchers.

Introduction

Modern molecular electronics suggests that the highly conjugated and strongly dipole-coupled molecular arrays can be utilized as molecular electronic and photonic wires, respectively.[1−12] The fabrication of long molecular arrays is indispensable for the connection between electrodes or energy donor and acceptor to achieve electrical conduction or energy transfer over a long distance.[13−15] To transfer charge or excitation energy over a long distance, it is of utmost importance to envisage well-arranged rigid molecular architectures. In this application, it is indispensable to minimize the energy or charge sinks, which may be formed by conformational heterogeneities in overall molecular structures, to realize high efficiency in energy and charge transport processes. In this regard, directly linked Zn(II) porphyrin arrays can be a promising candidate for a highly efficient molecular photonic wire due to strong dipole couplings between adjacent porphyrin planes arising from a close proximity. Elongation of conjugation through *meso*-carbon positions in longer porphyrin arrays induces electronic perturbations to produce a lot of conformers at ambient temperature.[16−19] Although a large steric hindrance between the directly linked porphyrin moieties minimizes the conformational change caused by the dihedral and tilt angle change between the two porphyrin planes, a summation of the dihedral angle distribution of ±15° at ambient temperature especially in long porphyrin arrays would give rise to a large variation in linear structures of long porphyrin arrays.[20,21] Electronic asymmetry in longer arrays is shown to influence significantly the nature of the observed excited state dynamics, driving unusual couplings of solvent-induced excited state and subsequent conformational relaxation processes that give rise to a time-dependent attenuation of the transition dipole moment.[16,17] As a consequence, we can expect that as the length of the porphyrin array increases, the conformer related relaxation is enhanced and the energy transfer efficiency decreases drastically. In this work, we have attempted to explore the effect of conformational heterogeneities of energy donor porphyrin arrays (***Zn***) on the excitation energy transport phenomena by using steady state and time-resolved fluorescence and absorption spectroscopy. For this purpose, we have employed directly *meso*−*meso* linked Zn(II) porphyrin arrays (***Zn***, Chart 1) and 5,15-biphe-

CHART 1

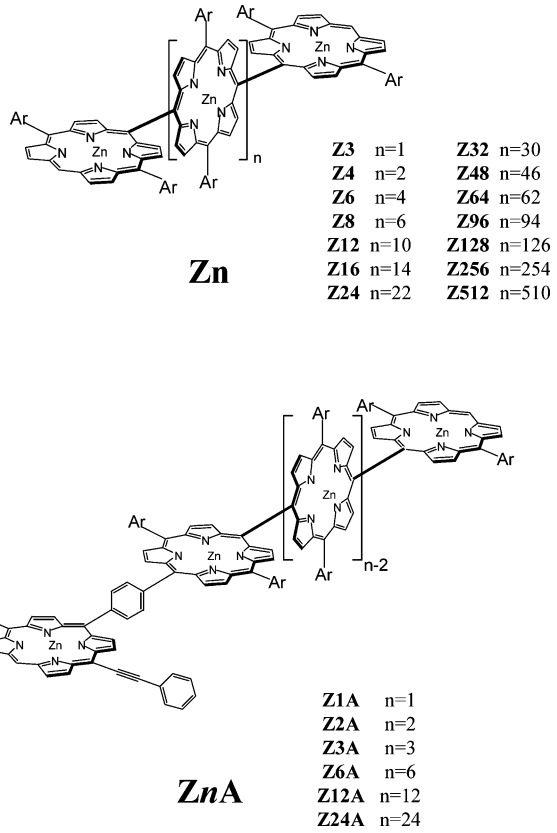

Zn

Z3	n=1	**Z32**	n=30
Z4	n=2	**Z48**	n=46
Z6	n=4	**Z64**	n=62
Z8	n=6	**Z96**	n=94
Z12	n=10	**Z128**	n=126
Z16	n=14	**Z256**	n=254
Z24	n=22	**Z512**	n=510

***Zn*A**

Z1A	n=1
Z2A	n=2
Z3A	n=3
Z6A	n=6
Z12A	n=12
Z24A	n=24

* To whom correspondence should be addressed. E-mail: osuka@kuchem.kyoto-u.ac.jp (A.O.); dongho@yonsei.ac.kr (D.K.).
† Yonsei University.
‡ Seoul National University.
§ Pohang University of Science and Technology.
|| Kyoto University.

10.1021/jp050662g CCC: $30.25
Published on Web 05/12/2005

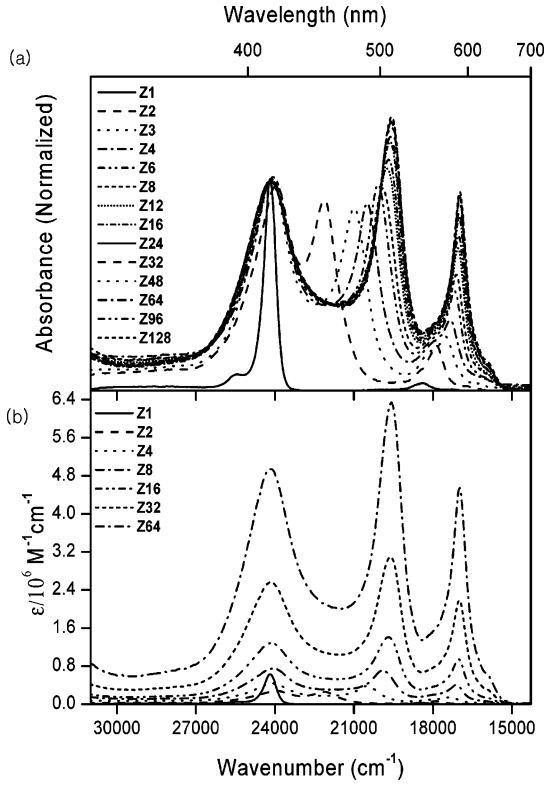

Figure 1. Series of steady state absorption spectra of the *meso*−*meso* linked porphyrin arrays (**Z*n*)** normalized at ∼24 000 cm^{-1} (a) and their molar extinction coefficient spectra (b) in THF.

nylethynylated Zn(II) porphyrin (acceptor **A**) linked to **Z*n*** arrays via a 1,4-phenylene spacer (**Z*n*A**, $n = 1$, 2, 4, 6, 12, and 24, Chart 1) at the *n*th *meso*-carbon of the *meso*−*meso* linked Zn(II) porphyrin donor array.[13] The triple bond linkage (ethynylated) at the two *meso* positions of the acceptor porphyrin moiety has an elongated π-conjugation pathway leading to the lowering of the excited electronic state of the acceptor. This feature enables **Z*n*A** to realize unidirectional energy transfer from the photoexcited donor array (**Z*n***) to the energy acceptor (**A**) upon reaching the terminal Zn(II) porphyrin unit attached to **A** in **Z*n*A** through excitation energy migration processes.

Results

Figure 1a shows the UV−visible absorption spectra of orthogonal porphyrin arrays (**Z*n***, Chart 1) in tetrahydrofuran (THF) normalized at ∼24 000 cm^{-1}. The Soret band splitting of **Z*n*** can be well described by exciton coupling theory.[22−26] The energy differences between high- and low-energy Soret bands become larger as the array becomes longer, showing asymptotic features ($\Delta E = \sim 4615$ cm^{-1}, Table 1).[27,28] On the other hand, the band shifts in the Q-bands are not so significant, showing a gradual increase in their intensities. The plot of the molar extinction coefficients of **Z*n*** as a function of the number of porphyrin units exhibits a linear summation behavior, indicating the higher absorptivity as the array becomes longer (Figure 1b).[27] In other words, each porphyrin moiety in the array can act as an independent light absorbing unit.

On the other hand, the fluorescence quantum yields of **Z*n*** increase up to **Z16**, which is followed by a continuous decrease in the fluorescence quantum yields as the array becomes longer than **Z16**. The decreased fluorescence quantum yields of longer porphyrin arrays than **Z16** indicate that each porphyrin unit in the array cannot act as an individual fluorophore.[27] The total fluorescence intensity decreases from **Z256** to **Z512**, but that

TABLE 1: Splitting Energies, Fluorescence Quantum Yields, Decay Lifetimes, and Anisotropy Values

model	ΔE^a (cm^{-1})	$\Phi_F{}^b$	$\tau_{avg}{}^c$ (ns)	$\tau_1{}^d$ (ns, %)	$\tau_2{}^e$ (ns, %)	r^f
Z1		0.022	2.64			0.008
Z2	2060	0.034	1.83			0.03
Z3	3176	0.044	1.72			0.05
Z4	3692	0.055	1.65			0.16
Z6	4104	0.066	1.59			0.21
Z8	4283	0.074	1.55			0.29
Z12	4434	0.080	1.52			0.31
Z16	4499	0.088	1.50			0.31
Z24	4557	0.083	1.43	1.49 (95.4)	0.14 (4.6)	0.27
Z32	4569	0.062	1.40	1.48 (92.8)	0.33 (7.2)	0.24
Z48	4595	0.058	0.93	1.47 (61.1)	0.08 (38.9)	0.20
Z64	4595	0.033	0.51	1.47 (31.2)	0.08 (68.8)	0.17
Z96	4615	0.031	0.50	1.45 (27.7)	0.14 (72.3)	0.13
Z128	4615	0.012	0.49	1.42 (21.8)	0.22 (78.2)	0.12
Z256	4615	0.012	0.40	1.05 (28.8)	0.14 (71.2)	0.12
Z512	4615	0.006	0.26	0.92 (17.7)	0.12 (82.3)	0.12

[a] Soret band splitting energy. [b] Fluorescence quantum yields. [c] Fluorescence decay lifetimes averaged with their ratios. [d] Longer fluorescence decay lifetimes with their ratios. [e] Shorter fluorescence decay lifetimes with their ratios. [f] Maximum values at fluorescence excitation anisotropy spectra.

TABLE 2: Fluorescence Data and EET Rate Constants

model	Φ_{EN}	$k_D{}^c$ (ps^{-1})	$k_A{}^d$ (ps^{-1})	R^f (Å)
Z1A	0.999^a			12.7
Z6A	0.76^b	35	35	33.6
Z12A	0.24^b	56	63	58.6
Z24A	0.085^b	110 ± 10	117^e	109

[a] EET rate constants calculated from $\Phi = 1 - \tau/\tau_{ref}$. [b] EET quantum yields based on the comparison of fluorescence spectra. [c] EET rate constants measured by time-resolved fluorescence decay profiles at 610 nm. [d] EET rate constants measured by time-resolved fluorescence rise profiles at 640 nm. [e] EET rate constant measured by a very weak fluorescence decay profile at 650 nm. [f] Center-to-center distances between the donor and the acceptor.

of **Z128** is similar to **Z256** (Table 1). The fluorescence decays of **Z*n*** also show a similar trend to the fluorescence quantum yields. As the porphyrin array becomes longer, the average fluorescence lifetimes of **Z*n*** decrease consistently up to **Z512** (Figure 2a). In the shorter arrays than **Z16**, the fluorescence decays exhibit single exponential behavior. On the other hand, as the array becomes longer than **Z16**, the fluorescence temporal profiles start to show double exponential decay in which the contribution by the fast decay component increases gradually as the array becomes longer up to **Z512** (Table 1 and Supporting Information S1). It should be noted that the fluorescence decay profiles depend on the probe wavelengths especially in **Z256** and **Z512** (Supporting Information S1). Specifically, as the probe

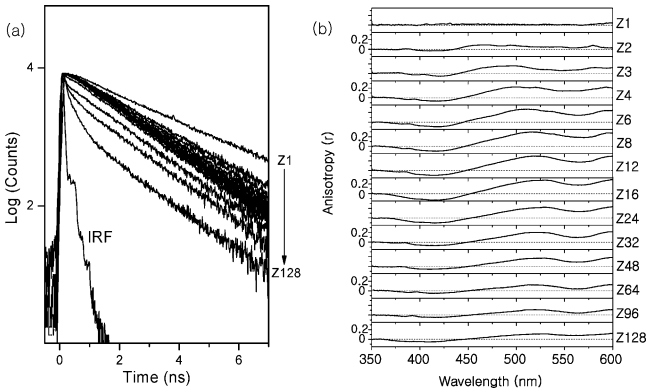

Figure 2. Series of fluorescence decay profiles of **Z*n*** (a) and steady state fluorescence excitation anisotropy spectra (b) in THF.

wavelength is shifted to red, the overall fluorescence decays become slower in **Z256** and **Z512**. In shorter arrays, however, the fluorescence decays do not show the probe wavelength dependence. This feature indicates that the excitation energy migration occurs from the initially excited shorter porphyrin oligomer segments to the longer ones, which is commonly observed in the photoexcitation dynamics of polymers.

In addition, we have recorded the fluorescence excitation anisotropy spectra of **Z*n*** to obtain information on the relative orientation between absorption and emission dipole arrangements in **Z*n*** (Figure 2b). The fluorescence excitation polarization of **Z1** is nearly $^1/_7$ regardless of the excitation wavelength, which is typical when both absorption and emission oscillators are degenerate and polarized in the same plane. In **Z*n***, however, were observed the negative anisotropy values in the fluorescence excitation anisotropy spectra around 413 nm which corresponds to the high-energy Soret band and the positive anisotropy values from 450 to 500 nm which corresponds to the low-energy Soret band, respectively.[27,28] The anisotropy values above ∼450 nm for **Z*n*** become larger and reach the maximum at **Z16** and then decrease in the arrays longer than **Z16** as the number of porphyrin units increases in **Z*n***. The maximum anisotropy value of ∼0.3 above ∼450 nm in **Z16**, which is still slightly smaller than 0.4 for the perfect in-plane orientation between absorption and emission dipoles, indicates a nearly parallel alignment between absorption and emission dipoles upon photoexcitation at the low-energy exciton split Soret and Q-bands. These features indicate that the overall geometries of **Z*n*** remain as the linear form when **Z*n*** is shorter than **Z16** and start to deviate from a linearity in overall geometry when the array is longer than **Z16**.

Systematic studies of excitation energy transfer (EET) processes in porphyrin arrays typically require the fabrication of assemblies that feature spectroscopically identifiable chromophoric entities that function as energy donor and acceptor. For this purpose, we have covalently attached highly conjugated 5,15-biphenylethynylated Zn(II) porphyrin as an energy acceptor (**A**) via a 1,4-phenylene spacer to the one end of the **Z*n*** array which can act as an energy donor,[13] where the electronic overlap between the **Z*n*** array and **A** is negligible due to the 1,4-phenylene spacer (**Z*n*A**, $n = 1$, 2, 3, 6, 12, and 24, Chart 1). As a result, the absorption spectrum of **Z*n*A** is a simple summation of the individual absorption spectrum of **Z*n*** (donor) and **A** (acceptor). This spectral feature enables us to excite selectively the **Z*n*** donor array to examine the energy flow from photoexcited **Z*n*** (donor) to ground state **A** (acceptor) by tuning the excitation wavelength to the absorption band of **Z*n*** (donor).

Figure 3 represents the normalized fluorescence spectra excited at their absorption maximum 414 nm of **Z6A**, **Z12A**, and **Z24A** and their corresponding reference arrays **Z6**, **Z12**, and **Z24** and the acceptor (**A**). The fluorescence spectrum of **Z6A** is nearly the same as that of **A** (acceptor), indicating that all the excited energy of donor is transferred to acceptor. On the other hand, the fluorescence spectra of **Z12A** and **Z24A** exhibit a hypsochromic shift relative to **Z6A** and a large similarity to their corresponding energy donor **Z12** and **Z24** arrays, suggesting that the energy donor arrays **Z12** and **Z24** contribute to the fluorescence spectra as a major emitter.

To estimate the EET efficiency, the fluorescence spectra of **Z*n*A** were reproduced by a quantitative summation of those of **Z*n*** and **A**. In shorter arrays than **Z4A**, their fluorescence spectra are nearly the same as that of **A**. After a fitting process, the relative emission ratios of the acceptor (**A**) in the **Z6A**, **Z12A**, and **Z24A** arrays were estimated to be 94.1, 86.8, and 43.2%, respectively (Figure 3). Considering their fluorescence quantum

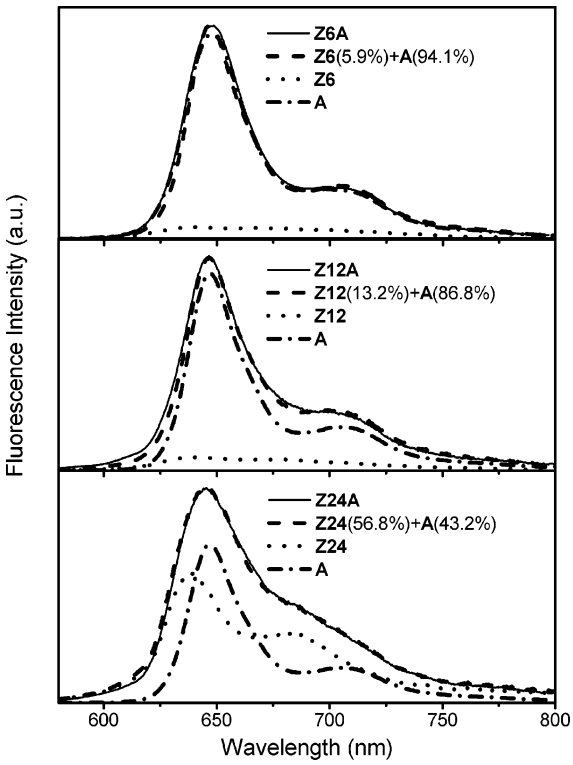

Figure 3. Normalized steady state fluorescence spectra excited at 414 nm of (a) **Z6A**, (b) **Z12A**, and (c) **Z24A** and their corresponding reference arrays (a) **Z6**, (b) **Z12,** and (c) **Z24** and the acceptor (**A**) in toluene. The fluorescence spectra of **Z*n*A** can be reproduced by a quantitative summation of those of **Z*n*** and **A**.

yields of 0.16, 0.044, and 0.031 for **Z6A**, **Z12A**, and **Z24A**, respectively, the fluorescence quantum yields of acceptors in those arrays can be calculated as 0.12, 0.035, and 0.013, respectively. Compared with the fluorescence quantum yield of 0.16 of the acceptor (**A**) only, we can estimate the energy transfer efficiencies in **Z6A**, **Z12A**, and **Z24A** to be 76, 24, and 8.5%, respectively. In other words, in **Z24A**, only 8.5% of the excitation energy is transferred from **Z24** to **A**. Therefore, the main energy relaxation process occurs within the donor array **Z24** before the excitation energy in **Z24** is transferred to the acceptor (**A**).

Figure 4 shows the fluorescence temporal profiles with fast (shorter than 120 ps) decay or rise component and long (∼1.6 ns) decay one at the fluorescence maxima of donor at 610 nm and acceptor at 640 nm. The fluorescence decay rates by the donor at 610 nm and the fluorescence rise rates by the acceptor at 640 nm are coincident with each other within our instrumental error. The obtained EET rates are $(35 \pm 3\ \text{ps})^{-1}$, $(60 \pm 4\ \text{ps})^{-1}$, and $(110 \pm 10\ \text{ps})^{-1}$ for **Z6A**, **Z12A**, and **Z24A**, respectively, which are in good accordance with the time-resolved transient absorption measurements.[13]

In the transient absorption measurements, however, we observed additional transient absorption decay processes which are not due to the EET processes (Figure 5). Specifically, the transient absorption decay profiles of **Z24A** at 510 nm after selective Q-band excitation at 588 nm of the donor array exhibit three relaxation processes with 2.7 ± 0.4 ps, 15 ± 2 ps, and 110 ± 10 ps time constants. While the relatively slow 110 ps component corresponds to the EET rate as observed in the time-resolved fluorescence measurements, the two additional 2.7 and 15 ps decay components are responsible for the solvent relaxation process and the conformational dynamics in **Z24A**, respectively (see the Discussion section). The fast decay with

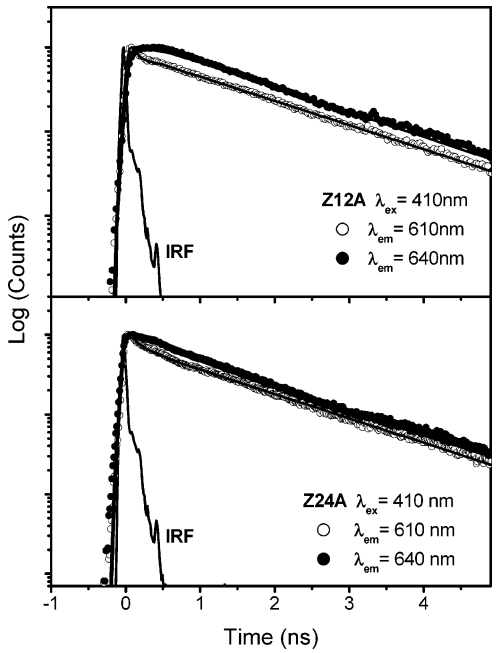

Figure 4. Fluorescence decay profiles at 610 nm (○) and 640 nm (●) of (a) **Z12A** and (b) **Z24A**.

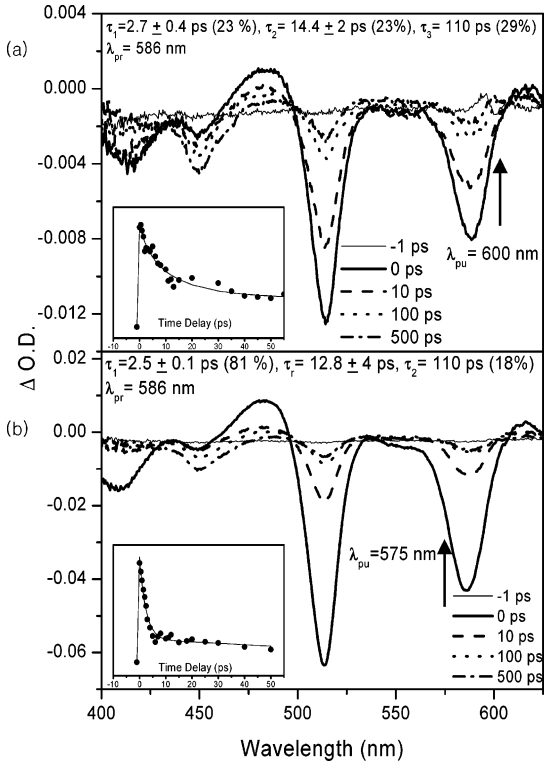

Figure 5. Hole burning transient absorption spectra of **Z24A** selectively excited at red (600 nm, (a)) and blue (575 nm, (b)) sides of the Q-band of the donor array **Z24**. The insets show temporal decay profiles probed at 588 nm in both excitations.

the time constant of 2.7 ps is similar to the experimentally observed solvent relaxation of toluene ($\tau = 2.72$ ps).[29] The other remaining component with a 15 ps time constant is largely consistent with the reported conformational dynamics such as ~8 ps for directly linked **Z2** dimer and 22−30 ps for ethyne-bridged Zn(II) porphyrin dimer.[16,30]

In addition, we carried out the spectral hole burning spectroscopy to investigate the conformational relaxation dynamics in **Z24A** by monitoring the transient absorption temporal profiles depending on the photoexcitation wavelength (Figure 5).[16,18] Selective excitation at both blue and red sides of the Q-band of the donor array **Z24** at 575 and 600 nm, respectively, exhibits different contributions of ~15 ps decay components in the overall transient absorption temporal profiles at 586 nm: 14 ± 2 ps decay and 12 ± 4 ps rise components in the cases of red and blue excitations, respectively. We also observed slight spectral bathochromic and hypsochromic shifts of ~2 nm or 50 cm^{-1} for blue and red excitations, respectively, in the course of transient absorption decay processes. We think that this shift corresponds to the energy difference between conformers existing in **Z24** at ambient temperature.[16,20,30]

Discussion

Conformational Heterogeneity of Zn(II) Porphyrin Arrays. The plot of molecular extinction coefficients of ***Zn*** indicates that the constituent porphyrin pigments can absorb light energy independently, which indicates a linear summation behavior in absorption intensity as the array becomes longer. On the other hand, in longer arrays than **Z16**, the fluorescence quantum yields gradually decrease. In addition, the fast fluorescence decay component abruptly appeared at **Z24**, and the contribution by the short component became larger, exhibiting a good correlation with a decrease in fluorescence quantum yield. In other words, in going from **Z16** to **Z24**, the fluorescence quantum yield decreases by about 5% and the contribution by the short component to the overall fluorescence decay of **Z24** increased by about the same ratio, which implies a close correlation between the fluorescence quantum yield and the contribution by the short component (Table 1). From these spectroscopic data, the conformational heterogeneity in longer arrays than **Z16** can be inferred, and the degree of heterogeneity increases as the array becomes longer. The conformational heterogeneities in longer porphyrin arrays are believed to arise from the dihedral angle distribution between adjacent porphyrin planes, which is ubiquitous in long peptide chains induced by the summation of dihedral angle change between adjacent amino acids.

To investigate the effect of flexibility of porphyrin arrays on the conformational heterogeneities, we have prepared more flexible Zn(II) porphyrin arrays by connecting **Z2** dimer units via a 1,4-phenylene bridge $\mathbf{(Z2)}_n$ (Supporting Information Chart S1). The overall absorption spectra of $\mathbf{(Z2)}_n$ linear arrays are characterized by the exciton split Soret bands due to a strong coupling in the constituent **Z2** units (Supporting Information Figure S4). As the number of **Z2** units increases in $\mathbf{(Z2)}_n$, so does the intensity of Soret bands, which is the same feature as observed in ***Zn***. On the other hand, the fluorescence quantum yields in $\mathbf{(Z2)}_n$ arrays reach the maximum value at $\mathbf{(Z2)_4}$ and then start to decrease monotonically as the $\mathbf{(Z2)}_n$ linear array becomes longer, which is also the same feature as observed in ***Zn*** (Supporting Information Table S2). A clear difference, however, is the early saturation in the fluorescence quantum yields in the $\mathbf{(Z2)}_n$ array compared with the ***Zn*** array, indicating that the enhanced structural distortion due to increased flexibility in the $\mathbf{(Z2)}_n$ array provides additional nonradiative channels in $\mathbf{(Z2)}_n$ compared with ***Zn*** (Supporting Information Figure S5). Consistently, the plot of fluorescence excitation anisotropy shows the maximum difference between the negative and positive anisotropy values in $\mathbf{(Z2)_4}$ in the series of the fluorescence excitation anisotropy spectra of $\mathbf{(Z2)}_n$ (Supporting Information Figure S5). In addition, the fluorescence lifetimes of $\mathbf{(Z2)}_n$ show a similar trend to that of ***Zn***, but the fluorescence decay of $\mathbf{(Z2)_1}$ was fitted as a double exponential decay

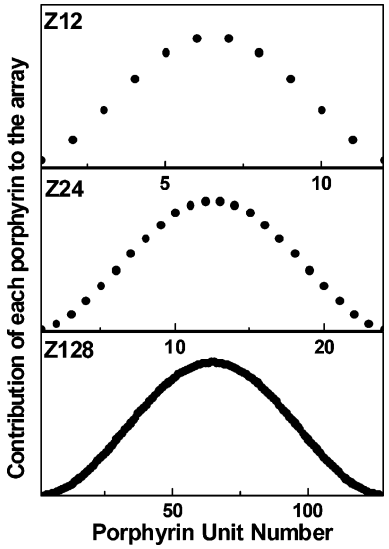

Figure 6. Contributions of each porphyrin unit to the excited exciton state of **Z12**, **Z24**, and **Z128** at each porphyrin unit calculated by the square of the coefficients from eq 1.

presumably due to conformers, suggesting the increased flexibility of the **(Z2)*n*** array. As the number of porphyrin pigments increases in **(Z2)*n***, the contribution by the fast decay component increases which is similar to the case of the **Z*n*** array (Supporting Information Table S3).

Excitation Energy Transfer Efficiencies of Z*n*A. In the **Z*n*A** system, the EET efficiency decreases significantly as the donor array length increases. More specifically, only 8.5% of the excitation energy in the donor array in **Z24A** is transferred to the acceptor. In other words, 91.5% of the excitation energy dissipates within the donor array.

Considering the electrostatic interaction between transition dipoles at neighboring porphyrins in the array, the excited state in the porphyrin array can be approximated as the exciton state.[13] When the energy donor array is composed of *N* porphyrins, the lowest exciton state in the array can be represented by

$$|d\rangle = \sqrt{\frac{2}{N+1}}\sum_{n=1}^{N}\sin\left(\frac{\pi}{N+1}n\right)|n\rangle \qquad (1)$$

where $|n\rangle$ represents a state of the array that the *n*th porphyrin therein is excited with a transition dipole parallel to the array while all the other porphyrins are unexcited.[13] From eq 1, the square of the coefficients represents the contribution of each porphyrin unit to the excited exciton state of the array. Figure 6 shows the contribution profiles of **Z12**, **Z24**, and **Z128**, in which the contribution exhibits the maximum value at the central porphyrin unit and decreases toward both ends in a sinusoidal manner. With the increased number of porphyrin units, the center-to-center distance increases between the acceptor porphyrin (**A**) located at the end of **Z*n*** and the donor array **Z*n***. The interesting point is that the summation of the excitation contribution for the four nearest porphyrin moieties corresponding to the S_1 state coherence length ($L = 4.5$ units, see the Supporting Information) in the **Z*n*** array reproduces well the observed energy transfer efficiencies of 77, 21, and 3.6% for **Z6A**, **Z12A**, and **Z24A**, respectively. In an analogous way, we can evaluate the very low EET efficiency of a longer energy donor array system like **Z128A** (0.028%) and the nearly unity EET efficiency within the exciton coupling domain size of energy donor array such as **Z1A**, **Z2A**, **Z3A**, and **Z4A**, since the number of porphyrin units in the energy donor array in these arrays is smaller than the evaluated coherence length of 4.5 units in the **Z*n*** array.

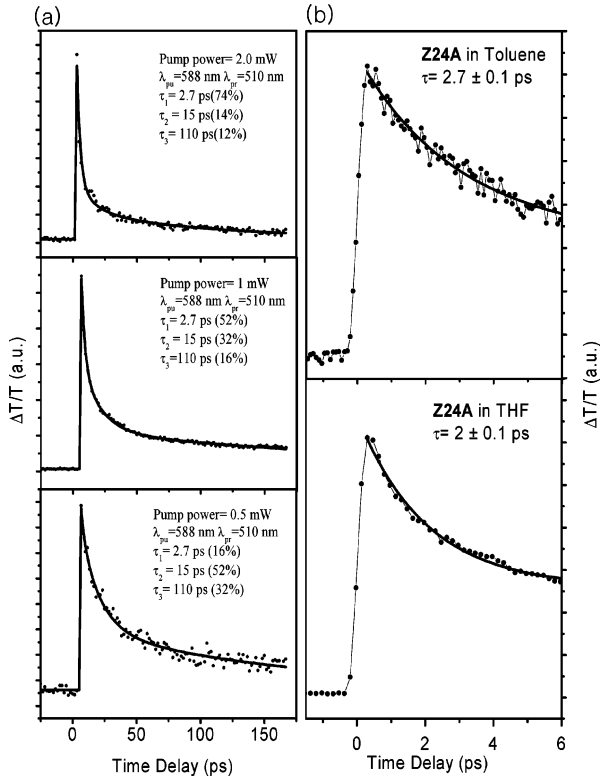

Figure 7. Temporal transient absorption profiles of **Z24A** in different excitation power (a) and different solvents (toluene and THF) (b) excited at 588 nm and probed at 510 nm.

Solvation Dynamics of Long Zn(II) Porphyrin Arrays. The low EET efficiency of **Z24A** indicates the unwanted energy relaxation process within the donor array. The main relaxation process observed in the transient absorption spectra of **Z24A** is the fast decay component with an ∼2−3 ps time constant throughout the visible region. The transient absorption decay profiles of **Z24** at 588 nm after selective Q-band excitation at 575 nm exhibit similar relaxation processes to **Z24A**: 2.7 ps, 14.5 ± 2 ps, and ∼1.5 ns (Supporting Information Figure S6). Except for the time constant corresponding to the EET process, all the components are nearly the same as those of **Z24A**, indicating that the major relaxation processes originate from the energy donor array **Z24**. The slowest decay process is presumably due to the S_1 state decay of **Z24**, as revealed by the fluorescence decay measurement.

One of the possible explanations for the fast decay component with a 2.7 ps time constant in **Z24** is a power-dependent process which can be described by the exciton−exciton annihilation process. As the porphyrin array length increases, just like the long polymer chain, the exciton−exciton annihilation process becomes manifest. To check this possibility, we decreased the excitation power to the extent of the lowest S/N ratio (Figure 7a). As the excitation laser power decreased, the contribution by this ultrafast process was diminished considerably but did not totally disappear. While this ultrafast process can be partially assigned to the exciton−exciton annihilation process, we cannot eliminate the other possibilities in the energy relaxation process of **Z24**. Next, the vibrational relaxation process can be assigned to this process. However, the vibrational cooling should be observed within a narrow spectral range. On the contrary, in **Z24A**, this ultrafast component was observed throughout the visible region including the acceptor bleaching band. The

vibrational cooling is the intrinsic molecular property which is rather insensitive to the nature of the solvent. Finally, to check the possibility of solvation dynamics, we measured the transient absorption decays in toluene and THF, revealing different ultrafast components of 2.7 ± 0.1 and 2.0 ± 0.1 ps, respectively (Figure 7b). These features are consistent with the reported results of 2.72 and 0.94 ps in toluene and THF, respectively, for coumarin 153 dye.[31] Consequently, we can conclude that the ultrafast relaxation component originates from the solvation dynamics in **Z24A**. Since the Franck−Condon state of the excited state generated by photoexcitation has a largely higher energy than the HOMO−LUMO gap, the solvent reorganization process initiates to stabilize the excess energy, and this process can be observed throughout the whole spectral range in the time-resolved transient absorption spectra.[31−34] Apparently, the excited states of the donor array in **Z12A** and **Z24A** undergo distortion, which was not observed in shorter arrays than **Z6A**. Porphyrin monomer does not exhibit the solvent related relaxation dynamics, in that it has a small Stokes shift in most organic solvents, because a large Stokes shift indicates the possibility of solvation relaxation. In longer **Z*n*** arrays in toluene and THF, however, the Stokes shift decreases gradually as the array length increases. This indicates that the hypsochromic shift in fluorescence is likely to be responsible for a decrease in the Stokes shift, which is due to the emissive heat sink with a higher energy than the HOMO−LUMO gap. As the porphyrin array increases, so does the size of its solvated shell, which increases the possibility of solvation dynamics.

Conformational Dynamics of Long Zn(II) Porphyrin Arrays. The hole burning spectroscopy has proven to be useful to probe the conformational dynamics in complicated molecular array systems. We chose excitation wavelengths of 575 and 600 nm to be in resonance with the blue and red sides of the Q-band maximum at 588 nm of **Z24**.[16] In the case of blue excitation, the ground state population of energetically lower conformers will be excited considerably. As the conformational population redistribution occurs, the bleached signal by the ground state will be recovered slowly. In the case of red excitation, conformers with higher energy are to be predominantly excited and exhibit the augmentation of the bleached absorption signal. Therefore, the bleaching recovery rate of the porphyrin donor array at the Q-band may represent the interconformer conversion rate. The $(\sim 15 \text{ ps})^{-1}$ component of the bleaching recovery signal in the transient absorption spectra can be assigned to the interconformer conversion rate. The spectral shift during the decay of the Q-band bleaching at 588 nm is estimated to be ~ 2 nm, or ~ 50 cm^{-1}, indicating that many conformers can exist at room temperature (~ 200 cm^{-1}). While the potential energy surface of the excited state would undergo various distortions due to numerous conformational local minima, the existence of conformers is mainly induced by the interporphyrin dihedral angle distribution. The ~15 ps decay component matches well with the conformational dynamics of ~8 ps for directly linked **Z2** and 22−30 ps for ethyne-bridged Zn(II) porphyrin dimer arising from the dihedral angle changes between the interporphyrin planes.[16,30] According to the theoretical calculation of directly linked porphyrin dimer **Z2**, the dihedral angle distribution of $90 \pm 15°$ is allowed at ambient temperature.[20] As the array length increases, so do the allowed dihedral angle distributions in the **Z*n*** array, which will change the electronic states of the adjacent porphyrin dimers in the array system. In addition, the reported scanning tunneling microscopy (STM) image of **Z48** shows a largely curved shape mainly because of tilt angle changes.[23] Consequently, the interporphyrin dihedral and tilt angle distributions give rise to conformational heterogeneity in the **Z*n*** array, resulting in the inefficient energy transfer from the photoexcited **Z*n*** array to the acceptor (**A**) especially in longer **Z*n*A** arrays.

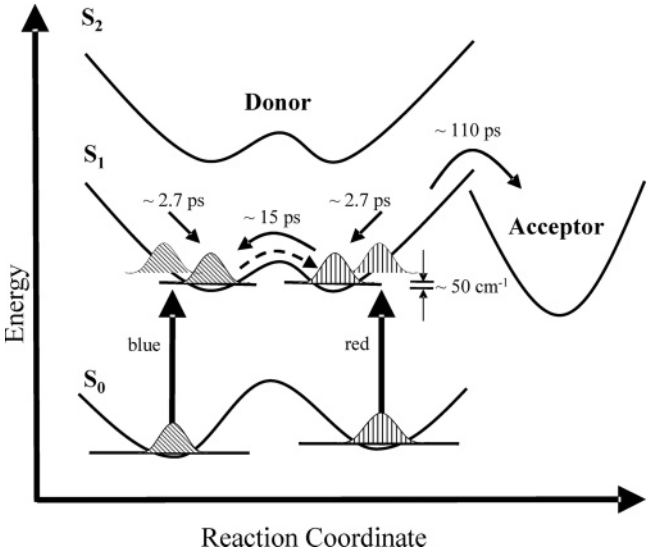

Figure 8. Schematic energy diagram of energy relaxation dynamics in **Z24A**.

To explain the overall energy relaxation dynamics occurring in **Z*n*A**, a schematic energy diagram is presented (Figure 8).[16,18] When a photon excites a molecule, a Franck−Condon state is produced and a relaxation process is simultaneously initiated. Because of the conformational heterogeneities, the potential energy surface of the first excited state (S_1) is more distorted than the ground state (S_0). Therefore, the solvent related relaxation process occurs (solvation dynamics). Meanwhile, owing to the interporphyrin conformational relaxation process involved in an ~15 ps time scale, only a small portion (~8.5%) of excitation energy is transferred to the acceptor (**A**) with the time scale of ~110 ps in **Z24A**.[13]

Conclusions

We have investigated the effect of conformational heterogeneities of long porphyrin arrays on the excitation energy transport phenomena by using time-resolved fluorescence and absorption spectroscopy. The conformational heterogeneities in longer porphyrin arrays influence significantly the nature of the observed excited state dynamics such as unusual couplings of solvent-induced excited state and subsequent conformational relaxation processes. The overall efficiencies of the EET processes in **Z*n*A** systems are diminished significantly especially when the energy donor array becomes longer to increase their absorptivities by increasing the number of porphyrin pigments in the **Z*n*** array. To minimize the conformational heterogeneity and improve the EET efficiency in longer molecular arrays, the construction of an LH1 type assembly, that is, circular array donor and central acceptor complex, could be a better way.[35] If the light-harvesting antenna is composed of the linear array, the pigments being farther than the coherence length should experience difficulties in the EET process to the reaction center, resulting in low energy transfer efficiency.

Experimental Section

Sample Preparations. *meso*−*meso* linked Zn(II) porphyrin arrays (**Z*n***, $n = 1$, 2, 3, 4, 6, 8, 12, 16, 24, 32, 48, 64, 96, and 128) were synthesized by the usual Ag^I-promoted coupling of

5,15-diaryl Zn(II) porphyrin **Z1**. Controlled NBS bromination of **Z*n*** (n = 1, 2, 3, 6, 12, and 24) gave a mixture of *meso*-bromo- and *meso*,*meso*-dibromo Zn(II) porphyrins. The *meso*-monobrominated porphyrins (**Z*n*B**, n = 1, 2, 3, 6, 12, and 24) were coupled with boronate Zn(II) porphyrin under Suzuki coupling conditions to furnish **Z*n*A** (n = 1, 2, 3, 6, 12, and 24). These model compounds have *meso*−*meso* linked Zn(II) porphyrin arrays as the energy donor and a 5,15-bisphenylethynylated Zn(II) porphyrin as the energy acceptor.[13]

Steady State Absorption and Fluorescence Measurements. Steady state absorption spectra were acquired with an UV−vis spectrometer (Shimazu, 1601A). Steady state fluorescence spectra were recorded on a fluorescence spectrometer (Hitachi, FL4500) and corrected with the comparison of the known chromophores. Steady state fluorescence excitation anisotropy spectra were obtained by changing the detection polarization on fluorescence path parallel or perpendicular to the polarization of exciting light. Then, anisotropy values were calculated as follows:

$$r = \frac{I_{VV} - GI_{VH}}{I_{VV} + GI_{VH}}$$

where I_{VV} (or I_{VH}) is the signal intensity when the excitation light is vertically polarized and only the vertically (or horizontally) polarized portion of the fluorescence is detected, denoting that the subscripts stand for excitation and detection polarization, respectively. The factor G is defined by I_{HV}/I_{HH} which is equal to the ratio of the sensitivities of the detection system for vertically and horizontally polarized light.[27,30] All solvents of HPLC grade were purchased from Aldrich and used without further purification. All measurements were carried out at ambient temperature.

Time-Resolved Fluorescence Decay Measurements. Time-resolved fluorescence was detected using a time-correlated single-photon-counting (TCSPC) technique.[36,37] As an excitation light source, we used a homemade cavity dumped Ti:sapphire oscillator which provided a high repetition rate (200−400 kHz) of ultrashort pulses (100 fs at full width at half-maximum (fwhm)) pumped by a CW Nd:YVO_4 laser (Coherent, Verdi). The output pulse of the oscillator was frequency-doubled with a second harmonic crystal. The TCSPC detection system consists of a microchannel plate photomultiplier (Hamamatsu, R3809U-51) with a cooler (Hamamatsu, C4878), a TAC (EG&G Ortec, 457), two discriminators (EG&G Ortec, 584 (signal) and Canberra, 2126 (trigger)), and two wideband amplifiers (Philip Scientific (signal) and Mini Circuit (trigger)). A personal computer with a multichannel analyzer (Canberra, PCA3) was used for data storage and processing. The overall instrumental response function was about 60 ps (fwhm). A sheet polarizer, set at an angle complementary to the magic angle (54.7°), was placed in the fluorescence collection system. The fittings for decays were performed by a least-squares deconvolution fitting process using the LIFETIME program with an iterative nonlinear least-squares deconvolution procedure developed at the University of Pennsylvania.[37]

Femtosecond Transient Absorption Measurements. The dual-beam femtosecond time-resolved transient absorption spectrometer consisted of a self-mode-locked femtosecond Ti:sapphire laser (Coherent, MIRA), a Ti:sapphire regenerative amplifier (Clark MXR, CPA-1000) pumped by a Q-switched Nd:YAG laser (ORC-1000), a pulse stretcher/compressor, an optical parametric generation and optical parametric amplification (OPG−OPA) system, and an optical detection system.[13,27,30] The amplified pulses were color-tuned by the optical parametric generation and optical parametric amplification (OPG−OPA) technique. The resulting laser pulses had a pulse width of ∼150 fs and an average power of 5−30 mW at a 1 kHz repetition rate in the range 550−700 nm. The pump beam was focused to a 1 mm diameter spot, and laser fluence was adjusted less than ∼1.0 mJ/cm^2 by using a variable neutral-density filter. The fundamental beam remaining in the OPG−OPA system was focused onto a flowing water cell to generate white light continuum, which was again split into two parts. The one part of the white light continuum was overlapped with the pump beam at the sample to probe the transient, while the other part of the beam was passed through the sample without overlapping the pump beam. The time delay between pump and probe beams was controlled by making the pump beam travel along a variable optical delay. The white continuum beams after sample were sent to a 15 cm focal length spectrograph (Acton Research) through each optical fiber and then detected by dual 512 channel photodiode arrays (Princeton Instruments). The intensity of the white light reaching each 512 channel photodiode array was processed to calculate the absorption difference spectrum at the desired time delay between pump and probe pulses. To obtain the time-resolved transient absorption difference signal at a specific wavelength, the monitoring wavelength was selected by using an interference filter. By chopping the pump pulses at 43 Hz, the modulated probe pulses as well as the reference pulses were detected by two separate photodiodes. The output current was amplified with a homemade fast preamplifier, and then, the resultant voltage signals of the probe pulses were gated and processed by a boxcar averager. The resultant modulated signal was measured by a lock-in amplifier and then fed into a personal computer for further signal processing.

Acknowledgment. This work has been financially supported by the National Creative Research Initiatives Program of the Ministry of Science & Technology of Korea. The work at Kyoto was supported by CREST (Core Research for Evolutional Science and Technology) of Japan Science and Technology Corporation (JST).

Supporting Information Available: Details of the synthesis; discussions on the coherence length (L) of orthogonal porphyrin arrays (**Z*n***) and on EET rates; figures showing spectral overlap and radiative rate constants, fluorescence decay profiles of **Z256** and **Z512**, absorption spectra of $(\mathbf{Z2})_n$ arrays, fluorescence decay profiles and fluorescence excitation anisotropy spectra of $(\mathbf{Z2})_n$, and transient absorption spectra of **Z24**; tables showing observed and calculated EET rate constants, fluorescence lifetimes of **Z256** and **Z512**, and Soret band splitting energies, fluorscence quantum yields, lifetimes, and anisotropy values of $(\mathbf{Z2})_n$; and chart showing the molecular structures of $(\mathbf{Z2})_n$. This material is available free of charge via the Internet at http://pubs.acs.org.

References and Notes

(1) Sundström, V.; Pulletis, T.; van Grondelle, R. *J. Phys. Chem. B* **1999**, *103*, 2327.

(2) Scholes, G. D.; Fleming, G. R. *J. Phys. Chem. B* **2000**, *104*, 1854.

(3) Hu, X.; Damhanovic, A.; Ritz, T.; Schulten, K. *Proc. Natl. Acad. Sci. U.S.A.* **1998**, *95*, 5935.

(4) van Oijen, A. M.; Ketelaars, M.; Köhler, J.; Aartsma, T.; Schmidt, J. *Science* **1999**, *285*, 400.

(5) Holten, D.; Bocian, D. F.; Linsey, J. S. *Acc. Chem. Res.* **2002**, *35*, 57.

(6) Debreczeny, M. P.; Svec, W. A.; Wasielewski, M. R. *Science* **1996**, *274*, 584.

(7) van der Boom, T.; Hayes, R. T.; Zhao, Y.; Bushard, P. J.; Weiss, E. A.; Wasielewski, M. R. *J. Am. Chem. Soc.* **2002**, *124*, 9582.

(8) Susumu, K.; Therien, M. R. *J. Am. Chem. Soc.* **2002**, *124*, 8550.
(9) Takahashi, R.; Kobuke, Y. *J. Am. Chem. Soc.* **2003**, *125*, 2372.
(10) *Molecular Electronics*; Jortner, J., Ratner, M. A., Eds.; International Union of Pure and Applied Chemistry, Chemistry for the 21st Century Monographs; Blackwell Science: Cambridge, MA, 1997; Chapter 1.
(11) Aratani, N.; Osuka, A.; Kim, Y. H.; Jeong, D. H.; Kim, D. *Angew. Chem., Int. Ed.* **2000**, *39*, 1458.
(12) Kim, D.; Osuka, A. *J. Phys. Chem. A* **2003**, *107*, 8791.
(13) Aratani, N.; Cho, H. S.; Ahn, T. K.; Cho, S.; Kim, D.; Sumi, H.; Osuka, A. *J. Am. Chem. Soc.* **2003**, *125*, 9668.
(14) Yoon, D. H.; Lee, S. B.; Yoo, K.-H.; Kim, J.; Lim, J. K.; Aratani, N.; Tsuda, A.; Osuka, A.; Kim, D. *J. Am. Chem. Soc.* **2003**, *125*, 11062.
(15) Cho, H. S.; Jeong, D. H.; Cho, S.; Kim, D.; Matsuzaki, Y.; Tanaka, K.; Tsuda, A.; Osuka, A. *J. Am. Chem. Soc.* **2002**, *124*, 14642.
(16) Rubtsov, I. V.; Susumu, K.; Rubtsov, G. I.; Therien, M. J. *J. Am. Chem. Soc.* **2003**, *125*, 2687.
(17) Shediac, R.; Gray, M. H. B.; Uyeda, H. T.; Johnson, R. C.; Hupp, J. T.; Angiolillo, P. J.; Therien, M. J. *J. Am. Chem. Soc.* **2000**, *122*, 7017.
(18) Kumble, R.; Palese, S.; Lin, V. S.-Y.; Therien, M. J.; Hochstrasser, R. M. *J. Am. Chem. Soc.* **1998**, *120*, 11489.
(19) Duncan, T. V.; Rubtsov, I. V.; Uyeda, H. T.; Therien, M. J. *J. Am. Chem. Soc.* **2004**, *126*, 9474.
(20) Yoshida, H.; Ishizuka, T.; Osuka, A.; Jeong, D. H.; Kim, D.; Matsuzaki, Y.; Nogami, A.; Tanaka, K. *Chem.—Eur. J.* **2003**, *9*, 58.
(21) Cho, H. S.; Song, J. K.; Ha, J.-H.; Cho, S.; Kim, D. *J. Phys. Chem. A* **2003**, *107*, 1897.
(22) Kasha, M. *Rev. Mod. Phys.* **1959**, *31*, 162.
(23) Kakitani, T.; Kimura, A. *J. Phys. Chem. A* **2002**, *106*, 2173.
(24) Kimura, A.; Kakitani, T.; Yamato, T. *J. Phys. Chem. B* **2000**, *104*, 9276.
(25) Bakalis, L. D.; Knoester, J. *J. Phys. Chem. B* **1999**, *103*, 6620.
(26) Mostovoy, M. V.; Knoester, J. *J. Phys. Chem. B* **2000**, *104*, 12355.
(27) Kim, Y. H.; Jeong, D. H.; Kim, D.; Jeong, S. C.; Cho, H. S.; Kim, S. K.; Aratani, N.; Osuka, A. *J. Am. Chem. Soc.* **2001**, *123*, 76.
(28) Ha, J.-H.; Cho, H. S.; Song, J. K.; Kim, D.; Aratani, N.; Osuka, A. *ChemPhysChem* **2004**, *5*, 57.
(29) To avoid the intermolecular aggregation effect of **Zn** which may reduce the fluorescence quantum yields, the spectroscopic experiments including steady state fluorescence, fluorescence decay, and fluorescence excitation anisotropy measurements were conducted in very dilute solutions (OD $\sim$ 0.1 in a 1 cm path length cell at an absorption maximum wavelength of 417 nm (Figure 2a)).
(30) Cho, H. S.; Song, N. W.; Kim, Y. H.; Jeong, S. C.; Hahn, S.; Kim, D.; Kim, S. K.; Yoshida, N.; Osuka, A. *J. Phys. Chem. A* **2000**, *104*, 3287.
(31) Reynolds, L.; Gardecki, J. A.; Frankland, S. J. V.; Horng, M. L.; Maroncelli, M. *J. Phys. Chem.* **1996**, *100*, 10337.
(32) Voth, G.; Hochstrasser, R. M. *J. Phys. Chem.* **1996**, *100*, 13034.
(33) Molotsky, T.; Huppert, D. *J. Phys. Chem. A* **2003**, *107*, 2769.
(34) *Activated Barrier Crossing*; Fleming, G. R., Hänggi, P., Eds.; World Scientific Publishing Co. Ltd.: Singapore, 1993; Chapter 7.
(35) Peng, X.; Aratani, N.; Takagi, A.; Matsumoto, T.; Kawai, T.; Hwang, I.-W.; Ahn, T. K.; Kim, D.; Osuka, A. *J. Am. Chem. Soc.* **2004**, *126*, 4468.
(36) Imahori, H.; Hosomizu, K.; Mori, Y.; Sato, T.; Ahn, T. K.; Kim, S. K.; Kim, D.; Nishimura, Y.; Yamazaki, I.; Ishii, H.; Hotta, H.; Matano, Y. *J. Phys. Chem. B* **2004**, *108*, 5018.
(37) Hwang, I.-W.; Cho, H. S.; Jeong, D. H.; Kim, D.; Tsuda, A.; Nakamura, T.; Osuka, A. *J. Phys. Chem. B* **2003**, *107*, 9977.